Chinese Physics Letters

LETTER

Symmetry-Enforced Single-Pair Charge-Two Triple-Point Semimetals

Cite as: Hui-Jing Zheng *et al*. 2026 *Chin. Phys. Lett.* **43** 100709

DOI CSTR

Recommended Articles

C-Type Antiferromagnetic Structure of Topological Semimetal $CaMnSb_2$

Bo Li *et al*.
Chin. Phys. Lett. **41**, (2024)

Rare-Earth-Tuned Evolution from d- to f-Orbital Dominance and Giant Anomalous Hall Effect in Topological *R*GaGe (*R* = Ce, Pr, and Nd) Semimetals

Zhian Xu, Jian Yuan, Ze Yan, Xia Wang, Na Yu, Shihao Zhang, and Yanfeng Guo
Chin. Phys. Lett. **43**, 060705 (2026)

Evolution of Topological Phases in Atomically Thin WTe_2 Films

Changcang Qiao, Chen-Chia Hsu, Tao Zhang, Zhiming Sun, Dong Qian, Yang-Hao Chan, and Peng Chen
Chin. Phys. Lett. **43**, 050702 (2026)

Physical Properties of RhGe and CoGe Single Crystals Synthesized under High Pressure

Shangjie Tian, Xiangjiang Dong, Bowen Zhang, Zhijun Tu, Runze Yu, Hechang Lei, and Shouguo Wang
Chin. Phys. Lett. **42**, 110708 (2025)

From Topological Nodal-Line Semimetals to Quantum Spin Hall Insulators in Tetragonal SnX Monolayers (X=F, Cl, Br, I)

Ye Zhu, Bao Zhao, Yang Xue, Wei Xu, Wenting Xu, and Zhongqin Yang
Chin. Phys. Lett. **41**, (2024)

Minimal Odd-Node Weyl-Dirac Complex and Strain-Induced Topological Phase Transition

Ze-Xin Xue, Ke-Xin Pang, Yun-Yun Bai, Yan-Feng Ge, Yan Gao, and Zhong-Yi Lu
Chin. Phys. Lett. **43**, 070708 (2026)

A series journal of Chinese Physical Society distributed by IOP Publishing

Chinese Physics Letters

Chin. Phys. Lett. **43** 100709 (2026)

LETTER

DOI: 10.1088/0256-307X/43/10/100709
CSTR: 32039.14.0256-307X.43.10.100709

Symmetry-Enforced Single-Pair Charge-Two Triple-Point Semimetals

Hui-Jing Zheng[1], Ke-Xin Pang[1], Yun-Yun Bai[1], Yan Gao[1,*], and Zhong-Yi Lu[2,3]

[1]State Key Laboratory of Metastable Materials Science and Technology & Hebei Key Laboratory of Microstructural Material Physics, School of Science, Yanshan University, Qinhuangdao 066004, China
[2]School of Physics and Beijing Key Laboratory of Opto-electronic Functional Materials & Micro-nano Devices, Renmin University of China, Beijing 100872, China
[3]Key Laboratory of Quantum State Construction and Manipulation (Ministry of Education), Renmin University of China, Beijing 100872, China

[*]Corresponding author. Email: yangao9419@ysu.edu.cn

The Nielsen–Ninomiya theorem mandates that the net chiral charge of topological nodes in a crystal's Brillouin zone must vanish, requiring them to appear in pairs. While realizing the absolute minimum of a single pair of topological nodes has been achieved for Weyl semimetals, hosting the minimal configuration of chiral charge-two ($|C| = 2$) triple-degenerate points (C-2 TPs) in a realistic electronic material remains an open challenge. By combining little-group constraints with both possible two-node orbit structures across all 1651 magnetic space groups (MSGs), we identify 21 MSGs without spin–orbit coupling (SOC) and 3 MSGs with SOC that are compatible with an isolated single pair of C-2 TPs. Guided by these symmetry criteria, we predict that the cubic boron allotrope $P23$-B_{36} acts as a premier electronic platform for this exotic phase. Owing to the negligible SOC of light boron atoms, the system behaves as a spinless semimetal, where the three crossing bands form exactly two symmetry-enforced C-2 TPs at the high-symmetry points Γ and R with chiralities $C = +2$ and $C = -2$, respectively. First-principles calculations reveal maximally extended double Fermi arcs on both the (001) and (110) surfaces, providing a distinct spectroscopic fingerprint for experimental detection. Our work establishes a rigorous symmetry-guided design framework for minimal multifold semimetals and identifies an elemental platform for exploring their intrinsic quantum transport phenomena.

Introduction

Topological semimetals hosting zero-dimensional band crossings have attracted immense interest because they realize emergent relativistic and non-relativistic quasiparticles protected by crystal symmetries [1−3]. In addition to Dirac and Weyl semimetals [4,5], crystal symmetries can stabilize unconventional multifold band crossings that host emergent fermionic excitations beyond those found in high-energy physics [6−8]. A prominent example is the triply degenerate point (TP), which represents a three-component band crossing intermediate between twofold degenerate Weyl and fourfold degenerate Dirac fermions [9−14]. Among the various classes of TPs, the chiral charge-two triple point (C-2 TP) is of particular interest as it carries a non-zero, quantized topological charge of $|C| = 2$ [14−17]. Hosting chiral pseudospin-1 fermions [18], C-2 TPs act as double-strength sources and sinks of Berry curvature, leading to unique physical effects such as super-Andreev reflection [14,19], supercollimation [20], and Klein tunneling [21].

Despite intensive searches, finding an ideal electronic material platform for C-2 TPs has been hindered by severe physical constraints. Previously predicted candidate materials, such as HfIrAs [22], $NaCu_3Te_2$ [23], and $PtBi_2$ [24], rely heavily on spin–orbit coupling (SOC) for band splitting. However, because SOC-induced band gaps are typically small, these TPs are easily disrupted by structural or thermal perturbations [25,26]. Furthermore, these materials fail to realize the "minimal nodal configuration", which represents the absolute lower bound of a single pair of topological nodes required to satisfy the Nielsen–Ninomiya theorem [27,28]. Instead, they exhibit multiple pairs of nodes or suffer from heavy band overlap with trivial bulk pockets, which severely contaminates the topological transport and boundary signatures [24,29,30]. Achieving a strictly isolated, single pair of C-2 TPs in a clean, SOC-free electronic system is therefore a highly sought-after yet unrealized objective.

In this Letter, we overcome this challenge by establishing the rigorous crystallographic design principles for the minimal C-2 TP configuration and predicting its realization in a light-element material. By screening both individually invariant nodes and symmetry-exchanged two-arm stars across all 1651 magnetic space groups (MSGs), we identify 21 MSGs without SOC and 3 MSGs with SOC that are compatible with an isolated single pair of C-2 TPs. The spinful candidates belong to magnetic Type-I and Type-III MSGs, whereas the nonmagnetic Type-II candidates occur only without SOC. This symmetry analysis guides us to the cubic boron allotrope $P23$-B_{36} (space group $P23$, No. 195). Because boron is a light element with negligible SOC, the system behaves as a spinless semimetal where a symmetry-enforced single pair of C-2 TPs is pinned exactly at the Γ and R points. Our first-principles calculations demonstrate that $P23$-B_{36} hosts a remarkably clean bulk band structure, with maximally extended double surface Fermi arcs on both the (001) and (110) surfaces. These features provide unambiguous spectroscopic fingerprints for experimental detection. Consequently, our work not only predicts the first ideal single pair of C-2 triple-point fermions in a spinless electronic system, but also provides a complete theoretical framework for the inverse design of the minimal single-pair C-2 TP configuration in both bosonic and spinless electronic systems.

Computational Method

First-principles electronic structure calculations were performed within the framework of density functional theory (DFT) as implemented in the Vienna *Ab initio* Simulation Package (VASP) [31]. The projector augmented-wave (PAW) method was employed to describe the ion–electron interactions [32], with the exchange-correlation energy treated under the generalized gradient approximation (GGA) of the Perdew–Burke–Ernzerhof (PBE) functional [33]. A

Received 14 July 2026; accepted 15 September 2026; published 2 November 2026
© 2026 Chinese Physical Society and IOP Publishing Ltd. All rights, including for text and data mining, AI training, and similar technologies, are reserved.

Check for updates

plane-wave basis set with a kinetic energy cutoff of 550 eV was used. The Brillouin zone (BZ) was sampled using a Γ-centered $6\times6\times6$ Monkhorst-Pack k-point grid [34]. The total energy and ionic force convergence criteria were strictly set to 10^{-6} eV and 10^{-3} eV/Å, respectively. Phonon dispersion spectra were calculated using the finite-displacement method implemented in the PHONOPY package [35], utilizing a $2\times2\times2$ supercell containing 288 atoms. The elastic stiffness constants C_{ij} were determined via the energy-strain relationship [36]. A Wannier tight-binding Hamiltonian was constructed using Wannier90 [37], with the boron 2s and 2p orbitals as the initial projections and a frozen energy window of $[-2,2]$ eV relative to the Fermi level. The resulting Hamiltonian was then used for topological calculations using WannierTools [38] package.

Symmetry Criteria for the Minimal Single-Pair C-2 TPs

To construct the minimal configuration of C-2 TPs, we establish the exact crystallographic prerequisites. Assuming two $|C|=2$ TPs are located at momenta $\boldsymbol{k}_1$ and $\boldsymbol{k}_2$ with little groups G_1 and G_2, the host MSG G must satisfy two constraints: (i) G must inherently host $|C|=2$ TPs. (ii) To avoid symmetry-induced node multiplication beyond two nodes, the two momenta must satisfy either: (a) each node is individually invariant under all operations of G, yielding $G_1=G_2=G$; or (b) the two nodes form a two-arm star ($\boldsymbol{k}$-star) related by an improper rotation $\mathcal{R}$ (including mirror, inversion, or rotoinversion) or the combined operation $\mathcal{R}\mathcal{T}$. In this case, the little cogroup $G_{\boldsymbol{k}_1}$ must be an index-2 subgroup of the parent point group G, i.e., $G=G_{\boldsymbol{k}_1}\cup\{\mathcal{R}\text{ or }\mathcal{R}\mathcal{T}\}G_{\boldsymbol{k}_1}$, where the coset operation reverses the chiral charge: $C(\boldsymbol{k}_2)=-C(\boldsymbol{k}_1)$.

By exhaustively screening the emergent-particle data [8,39,40] across all 1651 MSGs under both mechanisms, we find that an isolated single pair of C-2 TPs is allowed in 21 MSGs without SOC and in 3 MSGs with SOC, while no Type-IV MSG supports this phase. This complete classification is cataloged in Table 1 and Table SIII of the Supplementary Materials (SM). In the spinless regime without SOC, the minimal phase is allowed in eight Type-I (195.1, 197.7, 199.12, **204.30**, 207.40, 208.44, 211.56, 214.67), seven Type-II (195.2, 197.8, 199.13, 207.41, 208.45, 211.57, 214.68), and six Type-III (207.42, 208.46, 211.58, 214.69, **217.80**, **229.143**) MSGs. Remarkably, with SOC, it is uniquely realized at the P point in one Type-I (**206.37**) and two Type-III (**220.91**, **230.148**) MSGs under Mechanism (b). Under these symmetries, the C-2 TPs are enforced at the invariant high-symmetry points (HSPs) and transform according to three-dimensional irreducible (co)representations (IRRs) (e.g., R_4 or R_5), proving that this isolated state is highly rare and providing a direct guide for material discovery.

Crystal Structure and Stability of $P23$-B_{36}

Guided by our crystallographic symmetry criteria, we identify the light-element boron as a premier platform for hosting the spinless single-pair C-2 TP phase. Due to its light atomic mass, the intrinsic SOC of boron is exceptionally weak, allowing it to act as a virtual spinless electronic system. Furthermore, boron's propensity for multi-center covalent bonding enables the formation of diverse three-dimensional boron networks. Here, we predict a previously unreported cubic boron allotrope, $P23$-B_{36}, which crystallizes in the cubic space group $P23$ (No. 195), thereby satisfying the required symmetry criteria (see Table 1). The optimized lattice parameters are $a=b=c=7.92$ Å, where all 36 boron atoms occupy three inequivalent $12j$ Wyckoff positions (detailed coordinates are provided in Table SI of the SM).

The crystal structure of $P23$-B_{36} is composed of two distinct, interpenetrating structural motifs that build a robust three-dimensional framework [Figs. 1(a) and 1(b)]. The first motif consists of buckled

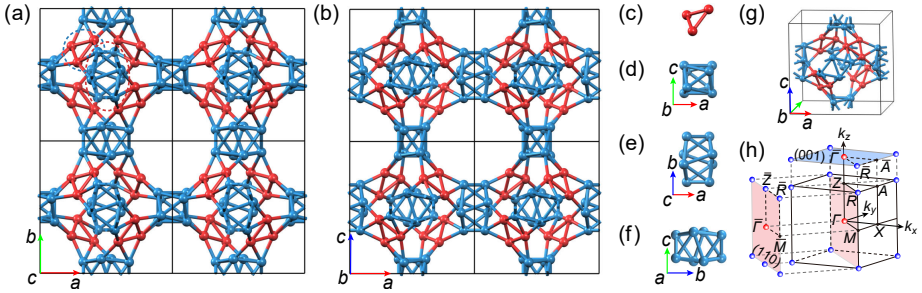

Fig. 1. Crystal structure and BZ of cubic $P23$-B_{36}. (a) Top view. (b) Side view in the a–c plane. (c) Buckled B_3 structural unit. (d)–(f) B_8 clusters systematically aligned along b, c, and a axes, respectively. (g) Primitive cell of $P23$-B_{36}. (h) Simple cubic BZ with TP_1 at Γ and TP_2 at R. Light blue and light red planes denote (001) and (110) surface projection surfaces and high-symmetry paths.

Table 1. Candidate MSGs among the 1651 MSGs that can host an isolated single pair of C-2 TPs with and without SOC. HSPs denote the high-symmetry points where the C-2 TPs are located. IRRs stand for the irreducible (co)representation of the little group at the HSPs [8,39,40]. Boldface entries indicate cases in which the single pair of C-2 TPs is related by an improper rotation ($\mathcal{R}$), where ($\mathcal{R}$) includes mirror, inversion, or rotoinversion operations, or by the combined operation $\mathcal{R}\mathcal{T}$. Detailed generators and (co)representations are provided in Table SIII of the SM.

Species	MSGs (HSPs)	Type of MSGs	IRRs
	Without SOC		
A single pair of C-2 TPs	195.1 (Γ, R); 197.7 (Γ, H, P); 199.12 (Γ, H); **204.30** (***P***)	I	$R/H(\boldsymbol{P})_4$
	207.40 and 208.44 (Γ, R); 211.56 and 214.67 (Γ, H)		R_4 or R_5
	195.2 (Γ, R); 197.8 (Γ, H)	II	R_4
	199.13 (Γ, H)		$\Gamma(R_4)$; $H(R_8)$
	207.41 and 208.45 (Γ, R); 211.57 (Γ, H)		R_4 or R_5
	214.68 (Γ, H)		$\Gamma(R_4;R_5)$; $H(R_9;R_{10})$
	207.42 and 208.46 (Γ, R); 211.58 (Γ, H, P); 214.69 (Γ, H); **217.80** (***P***); **229.143** (***P***);	III	$R(\boldsymbol{P})_4$
	With SOC		
	206.37 (***P***)	I	$\boldsymbol{P}_7$
	220.91 (***P***); **230.148** (***P***)	III	$\boldsymbol{P}_7$

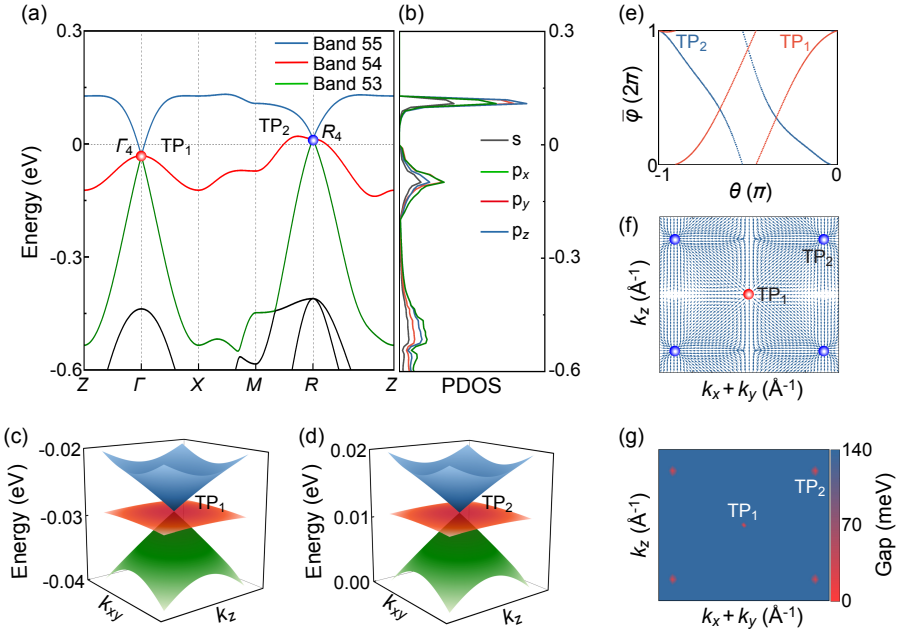

Fig. 2. Bulk band structure and topology of spinless $P23\text{-}B_{36}$. (a) Energy bands along high-symmetry paths. Red (TP_1 at Γ) and blue (TP_2 at R) dots denote threefold crossings of bands 53 to 55. (b) PDOS. (c) and (d) Three-dimensional dispersion showing linear energy splitting around TP_1 and TP_2. (e) WCC evolutions on closed spheres, giving topological charges $C = \pm 2$. (f) Berry curvature vector field in the $k_x + k_y - k_z$ plane, showing TP_1 as a source and TP_2 as a sink. (g) Global band-gap scan of the crossing bands across the BZ, showing an isolated single pair of C-2 TPs.

triangular B_3 units [Fig. 1(c)]. Within each unit cell [Fig. 1(g)], four of these B_3 triangles are aligned along the body diagonals, exhibiting a characteristic diagonal distribution. The second motif is formed by B_8 clusters [Figs. 1(d)–1(f)], which are ordered systematically along the three primary crystallographic axes (a, b, and c). These B_3 triangular clusters interpenetrate and couple with the network of B_8 octagonal rings, yielding a highly connected, rigid covalent framework.

The stability of the $P23\text{-}B_{36}$ phase is comprehensively validated. The calculated phonon spectrum exhibits no imaginary frequencies along the entire high-symmetry path of the BZ, confirming its dynamical stability (Fig. S1 in the SM). The computed elastic stiffness constants are $C_{11} = 106.91$ GPa, $C_{12} = 49.33$ GPa, and $C_{44} = 40.62$ GPa. These values satisfy the Born stability criteria for a cubic system [41]: $C_{11} - C_{12} > 0$, $C_{11} + 2C_{12} > 0$, and $C_{44} > 0$, yielding a bulk modulus of $B_0 = 68.52$ GPa. With a cohesive energy of -6.12 eV/atom, together with its robust covalent network and satisfaction of all structural, dynamical, and mechanical stability criteria, $P23\text{-}B_{36}$ is identified as a metastable boron allotrope.

Bulk Electronic Structure and the Single-Pair C-2 TP Phase

We next investigate the bulk electronic structure of $P23\text{-}B_{36}$. Due to the light atomic mass of boron, SOC is exceptionally weak, allowing us to describe the system under the spinless (without SOC) formalism with time-reversal symmetry $\mathcal{T}^2 = +1$. To rigorously verify this spinless approximation, we performed fully relativistic DFT calculations with SOC, as detailed in Fig. S3 of the SM. The relativistic band structure is virtually indistinguishable from the spinless result on the eV scale. Zooming into the crossing points reveals that finite SOC lifts the exact threefold degeneracies by opening minuscule avoided-crossing gaps of only $\Delta_{TP_1} = 0.36$ meV at Γ and $\Delta_{TP_2} = 0.013$ meV at R. Because these sub-meV gaps are negligible compared to both the bandwidth ($\sim$0.66 eV) and typical experimental resolutions on the order of meV, $P23\text{-}B_{36}$ serves as an ideal, effectively spinless platform. The spinful candidates in Table 1 belong to magnetic Type-I or Type-III MSGs, whereas nonmagnetic $P23\text{-}B_{36}$ belongs to Type-II MSG 195.2 and realizes the exact C-2 TP pair only in the no-SOC limit. The calculated bulk energy bands and the corresponding projected density of states (PDOS) are plotted in Figs. 2(a) and 2(b). The clear minimum in the PDOS at the Fermi level (E_F) confirms the semimetallic nature of the allotrope.

A systematic search of the band structures reveals that bands 53, 54, and 55 exhibit exactly two isolated threefold crossings in the entire BZ. The first triply degenerate point, TP_1, is situated at the Γ point at $E - E_F = -31$ meV, while the second point, TP_2, is located at the R point at $E - E_F = 13$ meV [Fig. 2(a)]. A global band-gap scan across the BZ [Fig. 2(g)] confirms that these three bands remain fully gapped elsewhere, thereby establishing a strictly isolated single pair of C-2 TPs.

For nonmagnetic $P23\text{-}B_{36}$ (Type-II MSG 195.2), both Γ and R are individually invariant under the full MSG, realizing case (ii-a). Their unitary little co-groups are the tetrahedral point group T, and the threefold degeneracies transform as Γ_4 and R_4, respectively. These real representations remain three-dimensional in the spinless time-reversal-symmetric setting and protect the local degeneracies. The isolated-pair configuration and opposite charges are established separately by the band search and the Wannier charge centers (WCC) calculations. Away from the HSPs, the three bands split linearly along all momentum directions [Figs. 2(c) and 2(d)], which is a hallmark of C-2 TP fermions.

To determine the topological charges of the nodes, we track the evolution of the WCC on closed spheres enclosing each C-2 TP [Fig. 2(e)]. For TP_1, the WCC curves wind twice along the positive direction, yielding a Chern number of $C = +2$. Conversely, for TP_2, the WCC curves wind twice in the negative direction, confirming $C = -2$. This topological charge is further visualized by the Berry curvature field distribution in the BZ plane containing both nodes [Fig. 2(f)]. The vector field illustrates that TP_1 acts as a source of Berry curvature, while TP_2 behaves as a sink. These monopoles satisfy the global neutrality condition required by the Nielsen–Ninomiya theorem in the simplest possible manner.

Low-Energy Effective $k \cdot p$ Model for the C-2 TPs in $P23\text{-}B_{36}$

To clarify the symmetry protection of the single-pair C-2 TPs, we first construct a low-energy $\boldsymbol{k} \cdot \boldsymbol{p}$ effective Hamiltonian at the Γ point.

The little group at Γ point is the point group T. Choosing the basis of the three-dimensional irreducible representation Γ_4, the representation matrices for the generators $C_{2,001}$, $C_{2,100}$, $C^{+}_{3,111}$, and the time-reversal symmetry $\mathcal{T}$ are expressed as

$$\mathcal{D}\{C_{2,001}\} = \begin{bmatrix} 1 & 0 & 0 \\ 0 & -1 & 0 \\ 0 & 0 & -1 \end{bmatrix}, \quad \mathcal{D}\{C_{2,100}\} = \begin{bmatrix} -1 & 0 & 0 \\ 0 & 1 & 0 \\ 0 & 0 & -1 \end{bmatrix}, \quad (1)$$

$$\mathcal{D}\{C^{+}_{3,111}\} = \begin{bmatrix} 0 & 0 & 1 \\ 1 & 0 & 0 \\ 0 & 1 & 0 \end{bmatrix}, \quad \mathcal{D}(\mathcal{T}) = \mathrm{I}_3\mathcal{K}, \quad (2)$$

where $\mathcal{K}$ is the complex conjugation operator. These operations constrain the effective Hamiltonian via

$$\mathcal{D}(g)\mathcal{H}(\boldsymbol{k})\mathcal{D}^{-1}(g) = \mathcal{H}(g\boldsymbol{k}), \quad (3)$$

where g represents the generators $\{C_{2,001}, C_{2,100}, C^{+}_{3,111}, \mathcal{T}\}$.

The spinless time-reversal symmetry, requiring $\mathcal{H}^{*}(\boldsymbol{k}) = \mathcal{H}(-\boldsymbol{k})$, dictates that the linear terms in $\boldsymbol{k}$ must be purely imaginary. Combined with Hermiticity, this restricts the linear Hamiltonian to an antisymmetric form. Solving Eq. (3) yields the linear three-band effective model

$$\mathcal{H}_{\mathrm{TP}_1}(\boldsymbol{k}) = \epsilon_0 + v \begin{bmatrix} 0 & \mathrm{i}k_y & -\mathrm{i}k_x \\ -\mathrm{i}k_y & 0 & \mathrm{i}k_z \\ \mathrm{i}k_x & -\mathrm{i}k_z & 0 \end{bmatrix} = \epsilon_0 + v\boldsymbol{k}\cdot\boldsymbol{J}, \quad (4)$$

where ϵ_0 is the energy of TP_1, v is the effective velocity, and J_i ($i = x, y, z$) are the spin-1 representation matrices,

$$J_x = \begin{bmatrix} 0 & 0 & 0 \\ 0 & 0 & -\mathrm{i} \\ 0 & \mathrm{i} & 0 \end{bmatrix}, \quad J_y = \begin{bmatrix} 0 & 0 & \mathrm{i} \\ 0 & 0 & 0 \\ -\mathrm{i} & 0 & 0 \end{bmatrix}, \quad J_z = \begin{bmatrix} 0 & -\mathrm{i} & 0 \\ \mathrm{i} & 0 & 0 \\ 0 & 0 & 0 \end{bmatrix}. \quad (5)$$

The eigenvalues of Eq. (4) are $E_0(\boldsymbol{k}) = \epsilon_0$ and $E_{\pm}(\boldsymbol{k}) = \pm v|\boldsymbol{k}|$, describing a flat band crossed by two linear dispersing bands. The dispersive bands carry Chern numbers $C = \pm 2$, where the Chern number of a nodal point is evaluated from the valence-band Berry flux through a small sphere enclosing the node, in agreement with the topological charges determined from the WCC calculations [Fig. 2(e)]. As illustrated in Fig. S2 of the SM, the optimized model parameters yield an excellent reproduction of the DFT bands, thereby corroborating the physical reliability of the effective model [42,43].

Meanwhile, because the little group at the R point is isomorphic to that at the Γ point, the R point shares the same symmetry protection and possesses the identical $\boldsymbol{k}\cdot\boldsymbol{p}$ effective Hamiltonian as Eq. (4). This unified effective model completely characterizes the low-energy excitations of our predicted minimal single-pair C-2 TP configuration.

Topological Surface States and Maximally Extended Double Fermi Arcs

The non-trivial bulk topology of $P23$-B_{36} is manifested on the boundaries via the bulk-boundary correspondence. Because the single-pair C-2 TPs carry quantized topological charges of $C = \pm 2$, their projected nodes on surfaces must be connected by exactly two topologically protected, widely extended surface Fermi arcs.

We calculate the surface-projected electronic states of $P23$-B_{36} on both the (001) and (110) surfaces. On the (001) surface, the surface bands display clear topological states bridging the projected bulk nodes [Fig. 3(a)]. In the constant-energy slice at $E - E_F = 13$ meV [Fig. 3(b)], we resolve two widely extended, exceptionally long double Fermi arcs that span the surface BZ to connect the projections of TP_1 and TP_2. This maximally extended double-Fermi-arc configuration constitutes a direct spectroscopic manifestation of the bulk $|C| = 2$ topological monopoles. A similar topological response is observed on the (110) surface [Fig. 3(c)]. At a constant-energy slice of $E - E_F = -31$ meV [Fig. 3(d)], a pair of widely extended double Fermi arcs is clearly resolved. The stable existence of these double Fermi arcs on two distinct crystallographic terminations confirms that these boundary states are robust topological features determined by the $|C| = 2$ bulk TPs, providing a clear spectroscopic fingerprint for experimental ARPES detection.

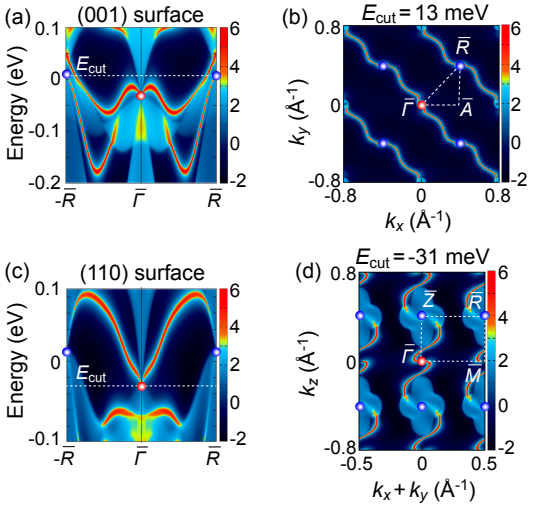

Fig. 3. Topological surface states and Fermi arcs of $P23$-B_{36}. (a) Surface bands on (001) projection. Dotted line marks $E - E_F = 13$ meV. (b) Maximally extended double Fermi arcs on (001) surface at 13 meV connecting projected bulk nodes. (c) Surface bands on (110) projection. Dotted line marks $E - E_F = -31$ meV. (d) Double Fermi arcs on (110) surface at −31 meV.

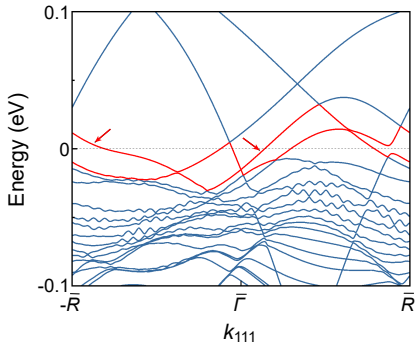

Fig. 4. Landau level dispersion along the k_{111} direction under $\boldsymbol{B} \parallel [111]$. Blue curves represent ordinary Landau bands. Red curves denote the pair of in-gap chiral Landau bands crossing the local gaps near Γ and R. The opposite group velocities ($v_g = \partial E/\partial k_{111}$) of the pairs at Γ ($v_g > 0$) and R ($v_g < 0$) correspond directly to the topological charges $C = \pm 2$, verifying the chiral anomaly of the single-pair TPs.

Landau Levels and Chiral Anomaly

To further verify the handedness of the single pair of C-2 TPs, we simulate the Landau level spectrum of $P23$-B_{36} under an external magnetic field applied along the [111] direction ($\boldsymbol{B} \parallel [111]$). Under this configuration, the threefold rotational symmetry $C_{3,111}$ is preserved, and the parallel momentum component k_{111} remains a well-defined quantum number, while the perpendicular electronic motion is quantized into discrete Landau bands [14,44].

The calculated Landau level spectrum along the $-R$–Γ–R path is shown in Fig. 4. The ordinary Landau bands are colored in blue, while the red curves highlight the topological in-gap states. Crucially, because each node carries a topological charge of $|C| = 2$, we observe

exactly a pair of chiral Landau bands crossing the local energy gap near both the Γ and R points. Around the Γ point ($C = +2$), the two chiral Landau bands disperse with a positive group velocity ($v_g = \partial E/\partial k_{111} > 0$), acting as a source of chiral charge. Conversely, around the R point ($C = -2$), the two chiral bands disperse with a negative group velocity ($v_g < 0$), acting as a sink. Under parallel electric and magnetic fields ($\boldsymbol{E} \parallel \boldsymbol{B} \parallel [111]$), this configuration drives an uncompensated chiral charge pumping between the two nodes, yielding a robust chiral anomaly and a strong negative longitudinal magnetoresistance.

Discussion and Conclusion

The prediction of $P23$-B_{36} as a spinless electronic platform hosting a single pair of C-2 TPs resolves several outstanding challenges in topological physics. First, unlike previously predicted transition-metal based triple-point semimetals that rely on narrow SOC gaps, the triple points in $P23$-B_{36} are protected strictly by the spatial symmetries of the space group $P23$. This spatial symmetry protection, combined with boron's negligible SOC, guarantees that the C-2 TPs remain stable. Second, the maximally extended double surface Fermi arcs are highly separated in momentum space and lie in a clean energy window near the Fermi level, making them excellent candidates for high-resolution ARPES observation without background interference.

Crucially, our work establishes a complete crystallographic classification of the 21 spinless MSGs that allow the minimal single-pair C-2 TP configuration. This classification also provides a symmetry-design guide for classical bosonic metamaterials (e.g., photonic, phononic, and acoustic crystals) when the relevant modes realize the single-valued corepresentations in Table 1. Distinct MSG types, however, dictate different physical platforms: while the seven Type-II MSGs (with bare time reversal $\mathcal{T}^2 = +1$) apply naturally to bosonic systems, the Type-I and Type-III MSGs require time-reversal-breaking or synthetic effective magnetic symmetries. Moreover, because bosonic bands do not have Fermi-level or electron-filling constraints, the target $|C| = 2$ TPs can be probed directly at their operating frequency. We emphasize that the MSG label provides a rigorous symmetry guide; however, establishing an exact single pair in a specific metamaterial requires verifying the IRRs, band connectivity, and the absence of extraneous crossings throughout the entire BZ.

In summary, we have established the theoretical design rules for the minimal configuration of charge-two TPs and predicted its realization in the previously unreported boron allotrope $P23$-B_{36}, opening a new avenue for exploring topological transport phenomena associated with unconventional multifold fermions in minimal node configurations.

Acknowledgments

This work was supported by the National Natural Science Foundation of China (Grant No. 12304202), the Hebei Natural Science Foundation (Grant No. A2023203007), and the Science Research Project of Hebei Education Department (Grant No. BJK2024085).

References

[1] Armitage N P, Mele E J, and Vishwanath A 2018 *Rev. Mod. Phys.* **90** 015001
[2] Bansil A, Lin H, and Das T 2016 *Rev. Mod. Phys.* **88** 021004
[3] Burkov A A 2016 *Nat. Mater.* **15** 1145
[4] Wan X, Turner A M, Vishwanath A, and Savrasov S Y 2011 *Phys. Rev. B* **83** 205101
[5] Young S M, Zaheer S, Teo J C Y, Kane C L, Mele E J, and Rappe A M 2012 *Phys. Rev. Lett.* **108** 140405
[6] Bradlyn B, Cano J, Wang Z, Vergniory M G, Felser C, Cava R J, and Bernevig B A 2016 *Science* **353** aaf5037
[7] Chang G, Wieder B J, Schindler F, Sanchez D S, Belopolski I, Huang S M, Singh B, Wu D, Chang T R, Neupert T, Xu S Y, Lin H, and Hasan M Z 2018 *Nat. Mater.* **17** 978
[8] Yu Z M, Zhang Z, Liu G B, Wu W, Li X P, Zhang R W, Yang S A, and Yao Y 2022 *Sci. Bull.* **67** 375
[9] Tian L, Liu Y, Yu W W, Zhang X, and Liu G 2021 *Phys. Rev. B* **104** 045137
[10] Zhu Z, Winkler G W, Wu Q, Li J, and Soluyanov A A 2016 *Phys. Rev. X* **6** 031003
[11] Weng H, Fang C, Fang Z, and Dai X 2016 *Phys. Rev. B* **93** 241202
[12] Lv B Q, Feng Z L, Xu Q N, Gao X, Ma J Z, Kong L Y, Richard P, Huang Y B, Strocov V N, Fang C, Weng H M, Shi Y G, Qian T, and Ding H 2017 *Nature* **546** 627
[13] Ma J Z, He J B, Xu Y F, Lv B Q, Chen D, Zhu W L, Zhang S, Kong L Y, Gao X, Rong L Y, Huang Y B, Richard P, Xi C Y, Choi E S, Shao Y, Wang Y L, Gao H J, Dai X, Fang C, Weng H M, Chen G F, Qian T, and Ding H 2018 *Nat. Phys.* **14** 349
[14] Feng X, Wu W, Huang Y, Yu Z M, and Yang S A 2021 *Phys. Rev. B* **104** 115116
[15] Hu Z, Jin L, Li C, Liu Y, Dai X, Zhang X, and Liu G 2024 *Phys. Rev. B* **110** 035152
[16] Chang G, Xu S Y, Wieder B J, Sanchez D S, Huang S M, Belopolski I, Chang T R, Zhang S, Bansil A, Lin H, and Hasan M Z 2017 *Phys. Rev. Lett.* **119** 206401
[17] Yang Y, Sun H X, Xia J P, Xue H, Gao Z, Ge Y, Jia D, Yuan S Q, Chong Y, and Zhang B 2019 *Nat. Phys.* **15** 645
[18] Tang P, Zhou Q, and Zhang S C 2017 *Phys. Rev. Lett.* **119** 206402
[19] Feng X, Liu Y, Yu Z M, Ma Z, Ang L K, Ang Y S, and Yang S A 2020 *Phys. Rev. B* **101** 235417
[20] Fang A, Zhang Z Q, Louie S G, and Chan C T 2016 *Phys. Rev. B* **93** 035422
[21] Shen R, Shao L B, Wang B, and Xing D Y 2010 *Phys. Rev. B* **81** 041410
[22] Song Z G, Felser C, and Sun Y 2018 *Phys. Rev. B* **98** 165131
[23] Wang J, Sui X, Shi W, Pan J, Zhang S, Liu F, Wei S H, Yan Q, and Huang B 2017 *Phys. Rev. Lett.* **119** 256402
[24] Gao W, Zhu X, Zheng F, Wu M, Zhang J, Xi C, Zhang P, Zhang Y, Hao N, Ning W, and Tian M 2018 *Nat. Commun.* **9** 3249
[25] Xia Y and Li G 2017 *Phys. Rev. B* **96** 241204
[26] Guo P J, Yang H C, Liu K, and Lu Z Y 2018 *Phys. Rev. B* **98** 045134
[27] Nielsen H B and Ninomiya M 1981 *Nucl. Phys. B* **185** 20
[28] Nielsen H B and Ninomiya M 1981 *Nucl. Phys. B* **193** 173
[29] Weng H, Fang C, Fang Z, and Dai X 2016 *Phys. Rev. B* **94** 165201
[30] Sun J P, Zhang D, and Chang K 2017 *Chin. Phys. Lett.* **34** 027102
[31] Kresse G and Furthmüller J 1996 *Comput. Mater. Sci.* **6** 15
[32] Blöchl P E 1994 *Phys. Rev. B* **50** 17953
[33] Perdew J P, Burke K, and Ernzerhof M 1996 *Phys. Rev. Lett.* **77** 3865
[34] Monkhorst H J and Pack J D 1976 *Phys. Rev. B* **13** 5188
[35] Togo A, Oba F, and Tanaka I 2008 *Phys. Rev. B* **78** 134106
[36] Le Page Y and Saxe P 2002 *Phys. Rev. B* **65** 104104
[37] Mostofi A A, Yates J R, Lee Y S, Souza I, Vanderbilt D, and Marzari N 2008 *Comput. Phys. Commun.* **178** 685
[38] Wu Q, Zhang S, Song H F, Troyer M, and Soluyanov A A 2018 *Comput. Phys. Commun.* **224** 405
[39] Liu G B, Zhang Z, Yu Z M, Yang S A, and Yao Y 2022 *Phys. Rev. B* **105** 085117
[40] Zhang Z, Liu G B, Yu Z M, Yang S A, and Yao Y 2022 *Phys. Rev. B* **105** 104426
[41] Mouhat F and Coudert F X 2014 *Phys. Rev. B* **90** 224104
[42] Zhang S, Sheng H, Song Z D, Liang C, Jiang Y, Sun S, Wu Q, Weng H, Fang Z, Dai X, and Wang Z 2023 *Chin. Phys. Lett.* **40** 127101
[43] Zhang Z, Yu Z M, Liu G B, Li Z, Yang S A, and Yao Y 2023 *Comput. Phys. Commun.* **290** 108784
[44] Zhao Y X and Yang S A 2021 *Phys. Rev. Lett.* **126** 046401